Journal Pre-proof

Bending of hard-magnetic soft beams: A finite elasticity approach with anticlastic bending

Aakila Rajan, A. Arockiarajan

PII: S0997-7538(21)00136-4
DOI: https://doi.org/10.1016/j.euromechsol.2021.104374
Reference: EJMSOL 104374

To appear in: *European Journal of Mechanics / A Solids*

Received date : 16 February 2021
Revised date : 15 June 2021
Accepted date : 19 July 2021

Please cite this article as: A. Rajan and A. Arockiarajan, Bending of hard-magnetic soft beams: A finite elasticity approach with anticlastic bending. *European Journal of Mechanics / A Solids* (2021), doi: https://doi.org/10.1016/j.euromechsol.2021.104374.

This is a PDF file of an article that has undergone enhancements after acceptance, such as the addition of a cover page and metadata, and formatting for readability, but it is not yet the definitive version of record. This version will undergo additional copyediting, typesetting and review before it is published in its final form, but we are providing this version to give early visibility of the article. Please note that, during the production process, errors may be discovered which could affect the content, and all legal disclaimers that apply to the journal pertain.

© 2021 Published by Elsevier Masson SAS.

Journal Pre-proof

Bending of hard-magnetic soft beams: a finite elasticity approach with anticlastic bending

Aakila Rajan[a,c], A Arockiarajan[b]

[a] *Department of Mechanical Engineering, Indian Institute of Technology Madras, Chennai 600036, India*
[b] *Department of Applied Mechanics, Indian Institute of Technology Madras, Chennai 600036, India*
[c] *Division of Engineering and Applied Science, California Institute of Technology, Pasadena, CA 91125, USA*

Abstract

Soft-materials that respond to external stimuli are very useful for application in soft robotics, stretchable electronics, biomedical applications etc. Recent times have seen a surge in research of magnetically activated polymers due to their wide range of material properties, applications and important features such as non-contact, fast and non-invasive actuation. Furthermore, these applications ask for Hard-magnetic particles, which can retain their magnetization even after the applied magnetic field has been removed. In this work, we focus on developing a thermodynamically-consistent analytical solution to the large bending deformation of hard-magnetic soft hyperelastic beams under the influence of an applied uniform magnetic field. The principal stress in the cross-sections, which arise due to anticlastic bending were also calculated. Lastly, a Prony series approximation was used to encapsulate the time dependent response of the material properties of the soft beam. The model was verified by comparing the results to previously developed experimental, numerical and analytical results.

Keywords: Hard-magnetic soft beams, Large deformation, Magnetic field, Anticlastic bending

1. Introduction

Recent times have seen a surge in the study of soft materials. These involve a wide range of materials such as photoactive materials [1, 2, 3, 4], magneto-active soft materials [5, 6, 7], pH-responsive polymers [8, 9], electro-active polymers [10], thermally activated polymers [11, 12, 13, 14] etc. Specifically, magnetically activated materials are of great interest due to their non-contact, fast and non-invasive actuation [15, 5, 16]. Magnetically activated polymers find much usage in bioengineering applications due to their biocompatibility, hydrophilic nature, non-toxicity, biodegradability, similar mechanical response as biological tissue and magnetic actuation [17]. The past decade has seen a wide range of research being conducted on magneto soft materials (elastomers and polymers) such as materials modelling [18, 6, 15, 19, 20, 21, 22], numerical simulations [19], synthesis [23, 24] and characterization [25, 23, 24].

Usually, these magnetically activated polymers are composed of a soft-matrix material embedded with ferromagnetic materials with low coercivity (called soft-magnetic particles) [26, 27]. Soft-magnetic particles are materials that are easily magnetized and demagnetized. They usually possess low coercivity (less than 1000 A/m). These materials are often used in applications where the material is magnetized in order to operate and then demagnetized after the operation, such as in the case of an electromagnet. A crucial limitation while dealing with soft-magnetic materials is the loss of their magnetism upon removing the external magnetic field due to their low coercivity [28, 29]. The application and usage of these soft-magnetic materials are quite limited as they have restricted movement and cannot undergo complex deformations. Therefore, to address these limitations, researchers have started using hard-magnetic materials. Hard-magnetic materials retain their magnetism even after the external magnetic field is removed. They have a coercive force greater than $10kA/m$. In order to completely demagnetize hard-magnetic particles, a very high opposite magnetic field is required. Embedding hard-magnetic particles into soft materials enables programmable and complex geometries under the influence of a magnetic field [30, 25]. These hard-magnetic soft-polymers have been actively used as soft robots

Email address: aarajan@iitm.ac.in (A Arockiarajan)

Journal Pre-proof

to navigate through complex and constrained environments, which can be used in various medical applications [25, 31, 32, 33].

To get a more fundamental understanding of these hard-magnetic soft materials, we require an understanding of their mechanical behaviour. The earliest known theoretical work on magneto coupled mechanical deformation was performed in the late 20th century [34, 35, 36]. Following these models, micro-mechanical modelling of the same materials was performed over 15 years ago [37, 38]. The continuum mechanics based models for magnetically activated soft materials is relatively more recent. The previous works by Saxena et al. proposed a continuum mechanics based model for magneto-viscoelasticity where a crucial assumption was made to split the applied magnetic field itself into elastic and viscous components [39]. The following work by Garcia-Gonzalez relaxed this assumption [28]. The article formulates a constitutive model for the finite deformation of soft material matrix with embedded hard-magnetic particles within a thermodynamically consistent framework. Viscous dissipation was coupled with hyperelasticity, and magnetic contribution to the mechanical behaviour through Maxwell's equations. The constitutive equations related the magnetic fields with the magnetic moments and stress components. The complete constitutive model was implemented into a finite element framework. Although the framework is valid for any hyperelastic energy function, the article is focused on a compressible Neo-Hookean model. The framework was applied to four numerical examples where the influence of the magnetic properties on the mechanical behaviour of smart structures was evaluated, namely (1) Uniaxial compression in an uniform constant magnetic field, (2) Uniaxial tensile test under varying magnetic fields, (3) Tests to observe the time dependent behaviour by varying magnetic and mechanical boundary conditions and (4) Inertial effects on uniaxial tensile tests under the influence of time dependent magnetic fields. Garcia-Gonzalez et al. [40] further modified the model which allowed diffusion of solvent across the polymer matrix. In the absence of any free current, the equilibrium equations and Maxwell's equations were coupled with mass conservation to account for variation in solvent concentration. The energy function was modified to include the viscous effects produced due to the solvent-polymer interactions [41]. The entire model was then implemented into a general FE framework.

Apart from theoretical modelling, significant experimental research for these hard-magnetic soft-materials was performed by Kim et al., where Hard-magnetic soft materials were synthesized by embedding neodymium-iron-boron (NdFeB) into polymeric gels [42]. Unlike soft magnetic materials, like pure iron, NdFeB has high coercivity and therefore, can preserve its magnetization once they are magnetically saturated. The primary matrix, in which these NdFeB particles are embedded, was synthesized by a soft elastomeric composite. Moreover, the research by Zhao et al. [5] presented a general magneto-elastic continuum-level framework to describe the deformation of such materials under external magnetic fields. Their model used additive decomposition of Cauchy stress tensor into magnetic and elastic components to couple the magnetic effects with deformation. This model was validated using experimental results of a beam embedded with hard-magnetic particle bending under a constant magnetic field [25, 5].

The primary limitation with all the above mentioned models is that such numerical models with finite element simulation requires high computational cost. Furthermore, these frameworks are not favourable for solving inverse problem in mechanics where calculating the magnitude of external magnetic field is of greater importance than predicting the future configuration with provided initial conditions. To overcome this limitation, Wang et al. proposed an analytical solution to hard-magnetic soft-beams under the influence a constant magnetic fields [29]. The analytical solution was also compared with numerical and experimental results [25, 5]. Although the proposed model can be used to predict and calculate the bending of the beam and the necessary magnetic field, the elastic contribution of the beam was modelled using a linearly elastic constitutive model. Furthermore, the model was primarily used to predict the behaviour of catheters coated with magnetic hydrogels. However, the model does not calculate the stresses across the beam's cross section, which is essential to observe the stresses in the underlying catheters. The variation of the principal stresses across the cross-sectional area of the catheter are important to compute localised stresses. The latest known research was presented by Chen et al. where they further expanded the model for functionally graded hard-magnetic linearly elastic beams [43]. The elastic modulus (E) of the entire material was approximated as

$$E = E_0 exp\left(\frac{2.5\psi}{1 - 1.35\psi}\right) \tag{1}$$

where E_0 is the modulus of an unadulterated elastomer without embedding the Hard-magnetic particle. ψ is the volume fraction of the hard-magnetic particle. But this research is also limited to pure linearly elastic

Journal Pre-proof

materials. Furthermore, as mentioned previously, the model fails to calculate the cross-sectional stresses, which are crucial for calculating the stresses in the underlying catheters.

To address this issue, a theoretical model has been developed to obtain the analytical solution for the bending of a hard-magnetic soft-beam under a constantly applied magnetic field. The hyperelasticity of the soft material has been captured using the Mooney-Rivlin constitutive model. The principal stresses have been calculated using an anticlastic bending approximation of the beam. Furthermore, Prony series has been used to incorporate the material property change due to relaxation. The model has been verified by comparing the results to previous experimental, numerical and analytical solutions. To reiterate, the novelty of this work is the derivation of an analytical solution for hard-magnetic soft hyperelastic beam bending under the influence of a constantly applied magnetic field [5]. The theoretical framework for deriving the necessary equations for hard-magnetic particles in a soft matrix was obtained by splitting the total Helmholtz energy into elastic and magnetic components. The constitutive model was verified to be thermodynamically consistent. The cross-sectional principal stresses which arise due to anticlastic bending was plotted for different cross-sections. These cross-sectional principal stresses are crucial for calculating localised stresses. The time dependent variation of the material parameters was also modelled using Prony series.

This manuscript has been organized as follows: Section 2 presents the theoretical model developed and the final analytical solution. Section 3 contains the results and comparison of the proposed model. Finally, section 4 concludes the study.

2. Theory

2.1. Continuum framework

The continuum framework presented in the works of *Wang et al* and *Garcia-Gonzalez* document a robust framework for soft materials containing hard magnetic particles [29, 28]. $\mathbf{X}$ and $\mathbf{x} = \chi(\mathbf{X})$ represents the material point in the reference and deformed configuration. χ is the deformation of the body. The deformation gradient is given by

$$\mathbf{F} = \mathrm{Grad}\mathrm{X} = \frac{\partial \mathrm{x}}{\partial \mathbf{X}} \tag{2}$$

The volumetric Jacobian is defined as $J = \det\mathbf{F}$. The beam contains hard-magnetic nano particles, whose magnetization vector is given by $\mathbf{M}$ vector and $\mathbf{m}$ vector in the reference and current configuration. Both the magnetization vectors are related by

$$\boldsymbol{\nabla}_{\mathbf{X}}\mathrm{M} = J\boldsymbol{\nabla}_{\mathbf{x}}\mathbf{m} \tag{3}$$

where $\boldsymbol{\nabla}_{\mathbf{X}}$ denotes the divergence in the reference configuration with respect to $\mathbf{X}$; while $\boldsymbol{\nabla}_{\mathbf{x}}$ denotes the divergence in the current configuration with respect to $\mathbf{x}$. Furthermore, Nanson's formula provides a relationship between the divergence of any vector (let's say $\mathbf{A}$) with respect to $\mathbf{X}$ and $\mathbf{x}$ [29]

$$\boldsymbol{\nabla}_{\mathbf{X}}\mathrm{A} = J\boldsymbol{\nabla}_{\mathbf{x}}(J^{-1}\mathbf{F}\mathbf{A}) \tag{4}$$

By combining equations (3) and (4), the relationship between $\mathbf{M}$ and $\mathbf{m}$ is

$$\mathbf{m} = J^{-1}\mathbf{F}\mathbf{M} \tag{5}$$

Helmholtz free energy measures the useful work obtainable from a closed system at constant temperature and volume. The derivative of this energy with deformation outputs the stress tensor. The elastic and magnetic component of the Helmholtz free energy per unit reference volume is a function of the deformation gradient: $\psi^{\mathrm{elastic}}(\mathbf{F})$ and $\psi^{\mathrm{magnetic}}(\mathbf{F}, \mathbf{B})$. The Helmholtz free energy density in the reference configuration can be additively decomposed into elastic and magnetic components

$$\psi(\mathbf{F}, \mathbf{B}) = \psi^{\mathrm{magnetic}}(\mathbf{F}, \mathbf{B}) + \psi^{\mathrm{elastic}}(\mathbf{F}) \tag{6}$$

For hyperelastic materials, the Piola stress ($\mathbf{P}$) and Cauchy stress tensor ($\boldsymbol{\sigma}$) are obtained by taking the derivative of the Helmholtz energy with $\mathbf{F}$

Journal Pre-proof

$$\mathbf{P} = \frac{\partial \psi}{\partial \mathbf{F}} \qquad \boldsymbol{\sigma} = J^{-1}\frac{\partial \psi}{\partial \mathbf{F}}\mathbf{F}^T \tag{7}$$

where $\mathbf{F}^T$ is the transpose of the deformation gradient tensor.

2.2. Balance Laws

The balance laws that need to be satisfied are the conservation of mass and momentum (linear and angular momentum). Since there is no material addition or deduction, mass is always conserved. The linear momentum balance must be satisfied everywhere in the deformed configuration to satisfy equilibrium condition:

$$\boldsymbol{\nabla}_{\mathbf{x}}.\boldsymbol{\sigma} + \mathbf{b} = 0 \tag{8}$$

$$\boldsymbol{\nabla}_{\mathbf{x}}.\boldsymbol{\sigma}^{\text{elastic}} + \mathbf{b}^m + \mathbf{b} = 0 \qquad \mathbf{b}^m = \boldsymbol{\nabla}_{\mathbf{x}}.\boldsymbol{\sigma}^{\text{magnetic}} \tag{9}$$

where $\mathbf{b}$ is the external mechanical body force vector. $\boldsymbol{\sigma}^{\text{elastic}}$ and $\boldsymbol{\sigma}^{\text{magnetic}}$ are the derivatives of $\psi^{\text{elastic}}(\mathbf{F})$ and $\psi^{\text{magnetic}}(\mathbf{F}, \mathbf{B})$ with $\mathbf{F}$ respectively. Equation (9) can be written in the reference configuration as

$$\boldsymbol{\nabla}_{\mathbf{X}}.\mathbf{P} + \mathbf{b}_0 = 0 \qquad \mathbf{b}_0 = J\mathbf{b} \tag{10}$$

$$\boldsymbol{\nabla}_{\mathbf{X}}.(\mathbf{P}^{\text{elastic}} + \mathbf{P}^{\text{magnetic}}) + \mathbf{b}_0 = 0 \tag{11}$$

We will show later that $\boldsymbol{\sigma}^{\text{magnetic}}$ and $\boldsymbol{\sigma}$ are asymmetric tensors (in equation (23) and (24)). The presence of magnetic dipoles combined with the application of an external magnetic field leads to the formation of body torques. Therefore, the conservation of angular momentum gives the equation for the body torque ($\boldsymbol{\tau}$)

$$\boldsymbol{\tau} = -\varepsilon : \frac{(\boldsymbol{\sigma} - \boldsymbol{\sigma}^T)}{2} = -\varepsilon : \frac{(\boldsymbol{\sigma}^{\text{magnetic}} - (\boldsymbol{\sigma}^{\text{magnetic}})^T)}{2} \tag{12}$$

where ε is the third-order permutation tensor and : is the double contraction operator of two tensors.
The Maxwell's equations in the absence of free current can be written as:

$$\boldsymbol{\nabla}_{\mathbf{X}} \times \mathbf{M} = \boldsymbol{\nabla}_{\mathbf{x}} \times \mathbf{m} = \mathbf{0} \tag{13}$$

$$\boldsymbol{\nabla}_{\mathbf{X}}.\mathbf{B}_0 = \mathbf{0} \tag{14}$$

where $\mathbf{B_0}$ is the magnetic flux density vector in the reference configuration. In this study, the magnetic field applied is assumed to be uniform; hence, Maxwell's equations are always conserved.

2.3. Constitutive equations

The elastic component of the Helmholtz free energy for soft materials has been taken from the works of [44].

$$\psi^{\text{elastic}} = aI_1 + bI_2 + cI_3 - \frac{d}{2}\ln I_3 \tag{15}$$

where a, b and c are positive material constants. The above form of the free energy is popularly known to capture the mechanical behaviour of a large class of soft materials. For zero pre-stress condition d must be equal to $d = 2(a + 2b + c)$ [44]. I_1, I_2 and I_3 are invariants of $\mathbf{F}$ given by

$$I_1 = ||\mathbf{F}||^2 \tag{16}$$

$$I_2 = ||(\text{det}\mathbf{F})\mathbf{F}^{-T}||^2 \tag{17}$$

$$I_3 = (\text{det}\mathbf{F})^2 \tag{18}$$

The deformation gradient $\mathbf{F}$, like any invertible second-order tensor, can be decomposed, using the polar decomposition theorem, into a product of two second-order tensors $\mathbf{F} = \mathbf{RU}$, where $\mathbf{R}$ is the rotation tensor and

Journal Pre-proof

U is the stretch tensor [45]. The Helmholtz free energy stored per unit volume (reference volume) due to an externally applied magnetic field (**B**)

$$\psi^{\text{magnetic}}(\mathbf{F},\mathbf{B}) = -\mathbf{FM}.\mathbf{B} \tag{19}$$

Equation (7) can be used to find the Piola-Kirchoff stress tensor from the Helmholtz energy

$$\mathbf{P} = \frac{\partial(\psi^{\text{elastic}}+\psi^{\text{magnetic}})}{\partial \mathbf{F}} \tag{20}$$

$$\mathbf{P} = 2\left(\frac{\partial\psi^{\text{elastic}}}{\partial I_1} + I_1\frac{\partial\psi^{\text{elastic}}}{\partial I_2}\right)\mathbf{F} - 2\frac{\partial\psi^{\text{elastic}}}{\partial I_2}\mathbf{BF} + 2I_3\frac{\partial\psi^{\text{elastic}}}{\partial I_3}\mathbf{F}^{-T} - \mathbf{B}\otimes\mathbf{M} \tag{21}$$

where $\mathbf{BF} = \mathbf{RU}^3$ and $\mathbf{F}^{-T} = \mathbf{RU}^{-1}$. The Cauchy stress tensor can be split into the magnetic and elastic contributions [28, 29].

$$\boldsymbol{\sigma} = J^{-1}\frac{\partial(\psi^{\text{magnetic}}+\psi^{\text{elastic}})}{\partial \mathbf{F}}\mathbf{F}^T \tag{22}$$

$$\boldsymbol{\sigma} = -J^{-1}\mathbf{B}\otimes\mathbf{FM} + J^{-1}\frac{\partial\psi^{\text{elastic}}}{\partial \mathbf{F}}\mathbf{F}^T \tag{23}$$

$$\boldsymbol{\sigma} = \boldsymbol{\sigma}^{\text{magnetic}} + \boldsymbol{\sigma}^{\text{elastic}} \tag{24}$$

The geometry of problem has been depicted in figure 1.

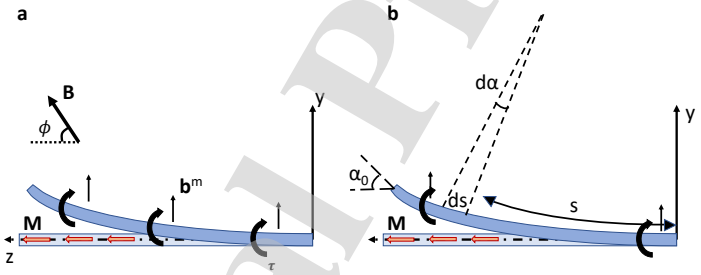

Figure 1: (a) Reference and deformed configuration of a hard-magnetic soft beam under the influence of an applied magnetic field **B**. **M** is the magnetization vector in the reference state. **B** and ϕ are the externally applied magnetic field and the angle between the field and **M**. $\mathbf{b}^{\text{m}}$ is the magnetic body force (as shown in equation 9) and $\boldsymbol{\tau}$ is torque (given in 12). (b) The deformed configuration of the beam under the applied magnetic field. α_0 is the the free-end angular displacement. The angle of bending as a function of the beam length is represented by $\alpha(s)$.

2.4. Anticlastic Bending

The configuration of the beam and the applied magnetic field has been depicted in figure 1. A cantilever beam composed of a soft hyperelastic material embedded with hard-magnetic particle has been deformed using a uniform magnetic field. Most research problems involving bending address it in a two-dimensional context and do not consider the bending in the third dimension (i.e. perpendicular to the bending plane). A two-dimensional assumption of the bending beam problem substantially reduces the complexity of the problem. Experimental evidence shows that a beam undergoing transversal deformation is always coupled with a longitudinal inflexion of a solid [46, 44, 47]. This phenomenon is termed as *Anticlastic Bending*. *Anticlastic bending* is the opposite curvature shown in the transverse direction, as opposed to the beam bending in the longitudinal direction when

Journal Pre-proof

a transverse load is applied on the beam. The effect has been shown artistically in figure 2. A technique to quantify the anticlastic bending can be obtained from the Poisson's ratio of the material [48]. Roughly speaking, the radius of curvature in the transverse direction would be the order of R_0/μ, where R_0 is the radius of curvature of the beam and μ is the poisson's ratio. Furthermore, the stresses which arise due to anticlastic bending can be compared with axial and bending stresses to judge their effect. A simple rule to deduce the magnitude of anticlastic bending might be difficult to judge in this sort of large deformations and can be explored in future works. A slender beam assumption is made here; hence the deformation preserves the planarity of cross-sections. Recently Lanzoni and Tarantino proposed a description of the displacement fields for beams undergoing anticlastic bending [44, 49]. We combine the displacement fields described with the current model for Hard-Magnetic Soft beams.

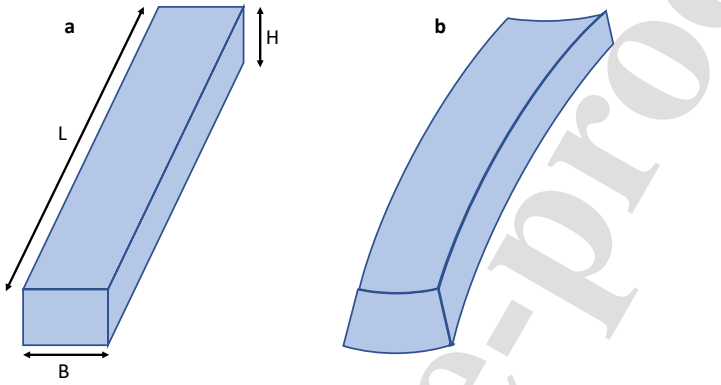

Figure 2: The figure represents the anticlastic bending effect in (a) undeformed configuration (b) deformed configuration [44]

The geometry of the deformation has been represented in figure 3. X, Y and Z are the global coordinates of the 3 dimensional space in the and $\tilde{x}, \tilde{y}$ are the local coordinate system of the cross section. α and β are the angles of rotation of the beam and rotation due to anticlastic bending. Similarly R_0 and r are the radius of curvature of the beam and cross sectional area. Here, both R_0 and r are a function of the material point on the beam (s), i.e. the radius varies along the beam. α_0 represents the maximum angle deflected by the beam. Correspondingly, β_0 is the maximum bending undergone in the transverse direction. Based on the previous observational data, the deformation is given by [49], [44]

$$x = re^{-\frac{Y}{r}} \sin\frac{X}{r} \tag{25}$$

$$y = -R_0 + \left(R_0 + r - re^{-\frac{Y}{r}} \cos\frac{X}{r}\right)\cos\frac{Z}{R_0} \tag{26}$$

$$z = \left(R_0 + r - re^{-\frac{Y}{r}} \cos\frac{X}{r}\right)\sin\frac{Z}{R_0} \tag{27}$$

where x, y and z are the material coordinates in the deformed configuration ($\mathbf{x}$). The displacement fields are derived using a semi-inverse approach in [49]. The deformation gradient for the above mentioned deformation is given by the product of the rotation tensor ($\mathbf{R}$) and stretch tensor ($\mathbf{U}$), $\mathbf{F} = \mathbf{RU}$. The rotation and stretch tensors are derived from the deformation defined in equation (27)

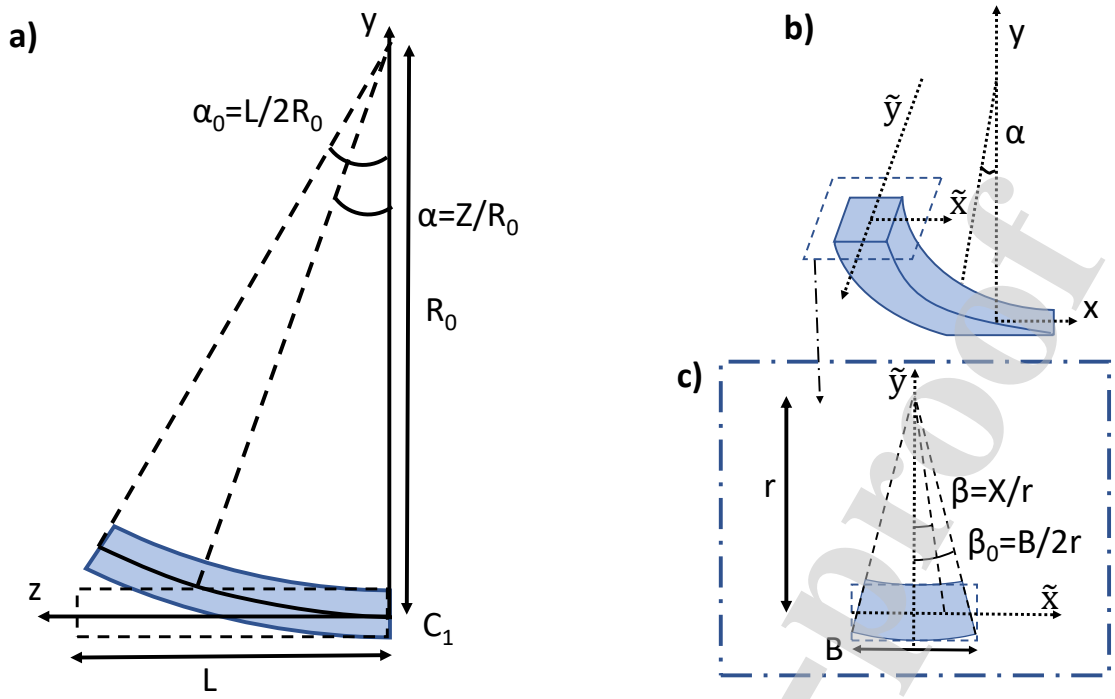

Figure 3: The image represents the deformation of a thin beam. Figure (a) shows the deformed configuration viewed from the vertical YZ plane and figure(b) shows the bending in transverse direction. Figure (c) shows the deformation of the cross sectional area [44].

$$\mathbf{R} = \begin{bmatrix} \cos\beta & -\sin\beta & 0 \\ \sin\beta\cos\alpha & \cos\beta\cos\alpha & -\sin\alpha \\ \sin\beta\sin\alpha & \cos\beta\sin\alpha & \cos\alpha \end{bmatrix} \tag{28}$$

$$\mathbf{U} = \begin{bmatrix} \lambda_X & 0 & 0 \\ 0 & \lambda_Y & 0 \\ 0 & 0 & \lambda_Z \end{bmatrix} \tag{29}$$

$$\lambda_X = \lambda_Y = e^{-\frac{Y}{r}} \tag{30}$$

$$\lambda_Z = 1 + \frac{r}{R_0}\left(1 - e^{-\frac{Y}{r}\cos\frac{X}{r}}\right) \tag{31}$$

where λ_X, λ_Y and λ_Z are the stretches in the X, Y and Z directions correspondingly. Notice that the centerline is given by $X = Y = 0$, which causes stretches in 3 directions to be 1. The Piola-Kirchoff stress given by equation 21 can be rewritten as [44]

$$\mathbf{P}^{\text{elastic}} = \mathbf{RS} \tag{32}$$

$$\mathbf{S} = \begin{bmatrix} S_X & 0 & 0 \\ 0 & S_Y & 0 \\ 0 & 0 & S_Z \end{bmatrix} \tag{33}$$

$$S_J = 2\left(\frac{\partial\psi^{\text{elastic}}}{\partial I_1} + I_1\frac{\partial\psi^{\text{elastic}}}{\partial I_2}\right)\lambda_J - 2\frac{\partial\psi^{\text{elastic}}}{\partial I_2}\lambda_J^3 + 2I_3\frac{\partial\psi^{\text{elastic}}}{\partial I_3}\frac{1}{\lambda_J} \qquad J = X, Y, Z \tag{34}$$

Journal Pre-proof

Journal Pre-proof

2.5. Solution

The parameters required to solve the entire system are $R_0(s)$ and $r(s)$. The conservation of momentum must satisfy equations (9), (11).

$$\mathbf{b}^m = \boldsymbol{\nabla}_{\mathbf{x}}.\boldsymbol{\sigma}^{\text{magnetic}} = J^{-1}(\boldsymbol{\nabla}_{\mathbf{x}}\mathbf{B})\mathbf{FM} \tag{35}$$

An important consideration of the hard-magnetic particles is that they are assumed to have a relative permeability close to 1. Since the magnetic field applied is homogeneous, and not affected by the magnetization of the beam, the spatial gradient of $\mathbf{B}$ is 0. Therefore, the conservation of momentum (11) contains another term $\boldsymbol{\nabla}_{\mathbf{X}}.\mathbf{P}^{\text{elastic}}$. Simplification of the equation yields three partial differential equations at the centerline ($X = Y = 0$) [44]

$$4\cos\frac{Z}{R_0}\frac{(b+c)r-(a+3b+2c)R_0}{rR_0} = 0 \tag{36}$$

For the expressions to satisfy equality along the centerline, we obtain the condition

$$r(s) = \frac{a+3b+2c}{b+c}R_0(s) \tag{37}$$

To find $R_0(s)$, we use a variational approach by minimizing the Helmholtz free energy [29]. The elastic component of the Helmholtz free energy, given by equation 15, can be approximated by

$$\psi^{\text{elastic}}(\alpha') = aI_1 + bI_2 + cI_3 - \frac{d}{2}\ln I_3 = \frac{E_{MR}I}{2A}\frac{1}{R_0^2} + \mathcal{O}\left(\frac{1}{R_0^6}\right) \approx \frac{E_{MR}I}{2AL^2}\left(\alpha'(s)\right)^2 \tag{38}$$

where $1/R_0$ is the longitudinal curvature, A and I are the cross-sectional area and area moment of inertia respectively. α' is the first derivative of α, i.e. $\alpha' = d\alpha(s)/ds$. E_{MR} is given by

$$E_{MR} = \frac{4(a+b)(a+4b+3c)}{a+3b+2c} \tag{39}$$

The rotation matrix ($\mathbf{R}$) along the centerline ($X = Y = 0$) has been given by

$$\mathbf{R} = \begin{bmatrix} 1 & 0 & 0 \\ 0 & \cos\alpha & -\sin\alpha \\ 0 & \sin\alpha & \cos\alpha \end{bmatrix} \tag{40}$$

The magnetic component of Helmholtz energy density can be expressed as

$$\psi^{\text{magnetic}}(\alpha, s) = -\mathbf{RM}.\mathbf{B} \tag{41}$$

The total Helmholtz free energy of the beam ($\prod$) will be written as:

$$\prod(\alpha(s)) = A\int_0^L \left(\psi^{\text{elastic}}(\alpha') + \psi^{\text{magnetic}}(\alpha, s)\right) ds \tag{42}$$

The equilibrium state can be found from the principle of stationary potential energy $\delta\prod = 0$, which yields Euler-Lagrange equation:

$$\frac{d}{ds}\left(\frac{\partial\psi}{\partial\alpha'}\right) = \frac{\partial\psi}{\partial\alpha} \tag{43}$$

$$\frac{d}{ds}\left(\frac{\partial\psi^{\text{elastic}}}{\partial\alpha'}\right) = \frac{\partial\psi^{\text{magnetic}}}{\partial\alpha} \tag{44}$$

$$\frac{E_{MR}I}{AL}\frac{d^2\alpha}{ds^2} = \frac{\partial}{\partial\alpha}\left(-\mathbf{RM}.\mathbf{B}\right) \tag{45}$$

Journal Pre-proof

It was shown in [29] that for a constant magnetic field at a certain angle (ϕ) to the beam ($i.e.\mathbf{B} = B\cos\phi\mathbf{e}_z + B\sin\phi\mathbf{e}_y$), equation (45) simplifies to

$$\boxed{\frac{E_{MR}I}{AL}\frac{d^2\alpha}{ds^2} + MB\sin(\phi-\alpha) = 0} \tag{46}$$

The method for solving the differential equation has been described in [29]. The above differential equation was further simplified into the following algebraic equation to obtain the free-end angular displacement (α_0).

$$\boxed{\sqrt{\frac{E_{MR}I}{2MBA}}\Phi(\phi,\alpha_0) - L = 0} \tag{47}$$

$$\Phi(\phi,\alpha_0) = \frac{2}{\sqrt{\cos(\phi-\alpha_0)-1}}\left\{F\left(\frac{\phi-\alpha_0}{2},\csc\left(\frac{\phi-\alpha_0}{2}\right)\right) - F\left(\frac{\phi}{2},\csc\left(\frac{\phi-\alpha_0}{2}\right)\right)\right\} \tag{48}$$

with function F referring to the first elliptic integral. Once the above equation is solved, the calculated α and R_0 can be used to calculate r and ultimately the cross-sectional stress patterns.

2.6. Time dependent response of material properties due to relaxation

The relaxation of material properties can describe any linear viscoelastic behaviour. Since hard-magnetic materials are embedded in soft materials, the material properties will have time-dependent responses. In our recent works, Prony series was used for viscoelastic materials to simplify their visco-hyperelastic behaviour [50]; therefore, we employ the same technique here. The Prony series can be well explained using a spring-dashpot model as shown in figure 4. Multiple parallel combinations of Maxwell models and a linear elastic spring is termed as Prony series.

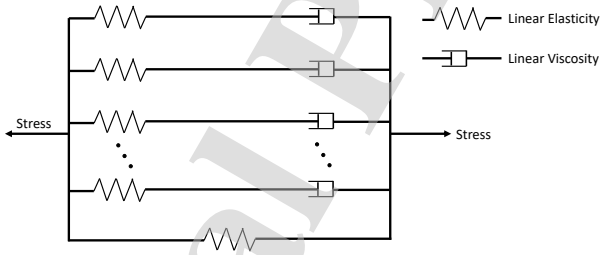

Figure 4: Spring-Dashpot phenomenological model for Prony series

Using the above model, The E_{MR} is equation (39) can be modified to

$$\frac{1}{E_{MR}} = J_0 + \sum_{i=1}^{m} J_i(1 - e^{-t/\tau_i}) \tag{49}$$

where J_i are the material compliance and τ_i are the relaxation time corresponding to the material compliance. t represents the time. Substituting this equation into the differential equation (47)

$$\boxed{\sqrt{\frac{I}{2MBA}\left(J_0 + \sum_{i=1}^{m} J_i(1 - e^{-t/\tau_i})\right)}\Phi(\phi,\alpha) - L = 0} \tag{50}$$

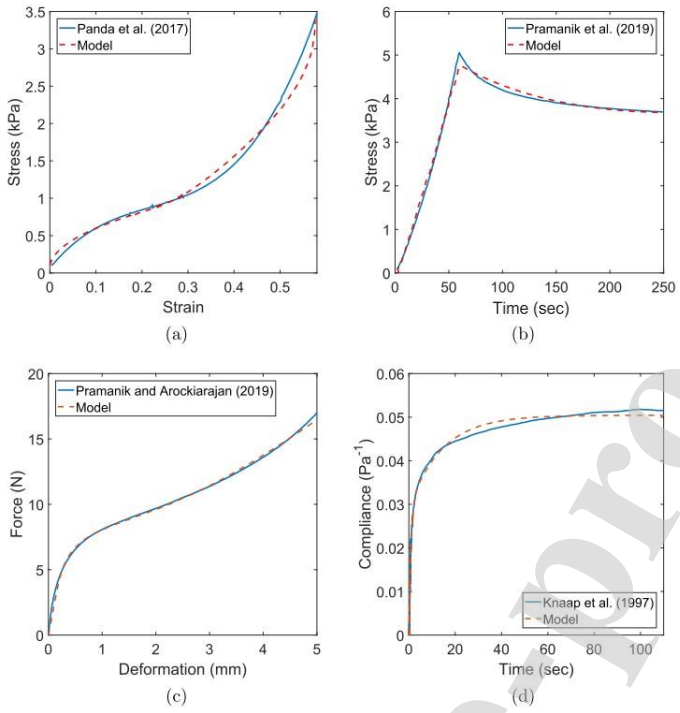

Figure 5: The figure represents the rationality of implementing Prony series to capture the material properties of soft materials. The experimentally obtained stress-strain plots for various types of soft materials were compared with Prony series approximation. (a) Panda et al performed uniaxial strain rate controlled tensile tests on hydrated silk fibroin sponges upto a strain of 0.6 [51] (b) Stress-relaxation test were conducted on polyvinyl alcohol xerogels containing nanocellulose crystals [52] (c) Transversely isotropic polyvinyl alcohol xerogels were uniaxially deformed along the fibre direction, and the force-deformation results were calculated [53] (d) Viscoelastic creep compliance shearing test was performed on collagen gels [54]. In all these scenarios, the Prony series approximation predicts the mechanical constitutive relation with good accuracy.

The angle at each material point changes with time. Past experimental data and observations have been employed to examine the accuracy of Prony series for modelling soft materials (refer figure 5). Our recent research [50] used the same Prony series approach to capture the time-dependent response of polymeric materials. The comparison between Prony series approximation of the material compliance and experimental stress-strain relations have been presented in figure 5. Figure 5 (a) presents the strain rate controlled uniaxial tensile tests on silk fibroin sponges [51]. The Prony series approximation predicts the stress well within the error range over the entire domain of strain. Similarly, figure 5 (c) shows the force-displacement plot for a transversely isotropic PVA-Xerogel; where compression was performed parallel to the fibre direction. Furthermore, as Prony series has been invoked to model the time dependent response of material parameters; we have shown its comparison with stress-relaxation tests on polyvinly alcohol xerogels in figure 5 (b) [52]. Finally, the Prony-series was directly compared to the time-dependent material compliance obtained from shearing test of collagen gels (figure 5) [54]. It is quite certain from the above mentioned examples that Prony series can be administered to soft materials in which Hard-magnetic particles are embedded due to its macro scale approach. The number of terms in the Prony Series depends on the material. The higher number of terms are always preferred to obtain the best prediction of the material behaviour. However, having higher terms leads to computational and experimental challenges. Constants involved in the Prony series expansion are determined by time dependent experiments such as creep and stress relaxation. Considering large number of terms in the expansion would require more experiments and complex curve-fitting algorithms. Generally two terms are sufficient to model viscoelasticity in polymeric materials [55, 50]. Since the material under consideration is a soft matrix, we have also considered two terms in the Prony series expansion.

Journal Pre-proof

Journal Pre-proof

2.7. Thermodynamic Considerations

First and second law of thermodynamics can be satisfied together by veryifying the Clasuis-Duhem Inequality-

$$T\dot{s} - \dot{u} + \boldsymbol{P}\dot{\boldsymbol{F}} - \frac{1}{T}q\nabla T \geq 0 \tag{51}$$

where $\dot{s}$ and $\dot{u}$ are the rate of change of entropy and internal energy per unit mass with respect to time. q is the heat flux vector per unit area and T is the temperature. From the fundamental equation of thermodynamics, we can write the total Helmholtz free energy density mentioned in equation (6) as

$$\psi = u - Ts \tag{52}$$

Therefore, we can write equation (51) as

$$\underbrace{(T\dot{s} - \dot{u})}_{=\dot{\psi}} + \boldsymbol{P}\dot{\boldsymbol{F}} - \frac{1}{T}q\nabla T \geq 0 \tag{53}$$

Since there is no heat or temperature gradient, the last term in the equation vanishes.

$$-\underbrace{\dot{\psi}}_{=\frac{\partial\psi}{\partial F}\dot{\boldsymbol{F}}} + \boldsymbol{P}\dot{\boldsymbol{F}} \geq 0 \tag{54}$$

$$\boldsymbol{P}\dot{\boldsymbol{F}} - \frac{\partial\psi}{\partial F}\dot{\boldsymbol{F}} \geq 0 \tag{55}$$

$$\left(\boldsymbol{P} - \frac{\partial\psi}{\partial F}\right)\dot{\boldsymbol{F}} \geq 0 \tag{56}$$

since $P = \frac{\partial\psi}{\partial F}$ (refer to equation (7)), the first and second law of thermodynamics are satisfied.

3. Results

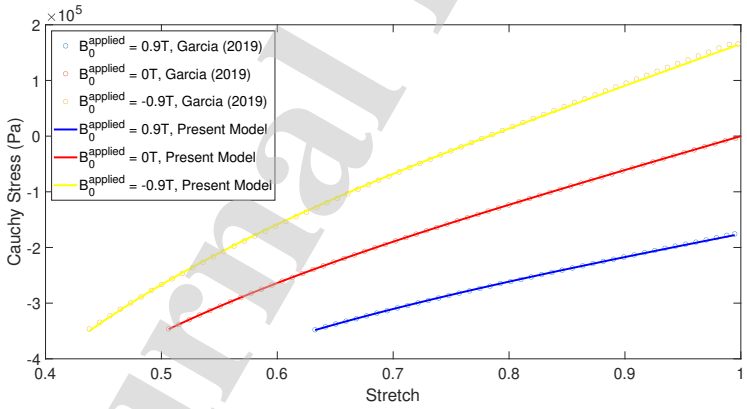

Figure 6: The image depicts the comparison of the developed framework and [28]. Different values of external magnetic field was applied ($\mathbf{B}_0^{\text{applied}}$) and the stress values were plotted against the stretch. Garcia (2019) represents the numerical simulation in [28] and the present model representing the curves derived through the current model.

The validity of the continuum framework can be verified by comparing it with previously developed hard-magnetic soft material models [28]. Garcia-Gonzalez et al. conducted a numerical simulation of a cubic sample of soft matrix containing Hard-magnetic particles, being uniaxially compressed under the influence of an applied magnetic field. The compression takes place until a certain stress value is reached in the material. Consequently, the required stretch to reach the desired stress can be modified by applying a different magnetic field. The

solution for the above problem obtained using our developed framework was compared with the results by Garcia-Gonzalez et al. [28]. The stress-stretch curves were calculated for compression loading under three values of external magnetic fields ($\mathbf{B}_0^{\text{applied}}$, i.e. varying values of $\mathbf{B}$ in equation 47).

The stress-stretch curves for the deformed configuration has been shown in figure 6. The sample is compressed until the stress reaches the value of $\sigma = -350kPa$. This means a constant magnetic stress contribution is present. Therefore, the total stress depends upon the magnetic field actuating the material. Furthermore, at stretch $= 1$, we can see that the stress in the materials is varying with change in the magnetic field applied. At this point, the Cauchy stress is only due to the magnetic contribution (since the elastic stress contribution is 0) as the material is relaxed and has no extension or compression. It is clear from figure 6 that the present model described in this paper can predict the numerical solutions to the same problem calculated in the works of Garcia et al. [28].

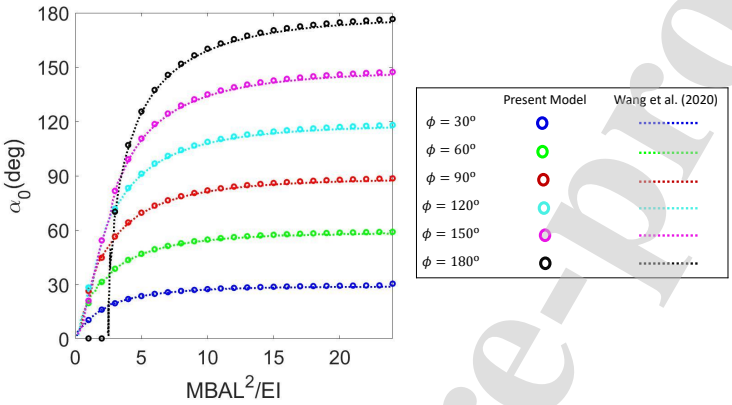

Figure 7: The graph presents the free-end angular displacement (α_0) against normalized magnetic field $MBAL^2/E_{MR}I$. The dotted lines represent the results presented in [29] and the circle markers are the solutions for the equation (48).

The geometry considered in the problem (as represented in figure 1) has been chosen specifically to compare the experimental results presented in the works of *Wang et al.* and *Zhao et al.* [29, 5]. A soft cantilever beam contains hard magnetic nanoparticles suspended within the material. This causes the material to become magnetically active. When it is kept within a constant magnetic field, the material will develop a body force and torque, causing it to deform. The field is strong enough that it does not get affected by the magnetic field possessed by the nanoparticles, but is not stronger than the coercivity of the same nanoparticles. We can solve equation (48) for the free-end angular displacement (α_0), given material properties and applied magnetic field vector. The maximum angle of deflection of the beam (α_0 in figure 6) can be calculated using equation 48. Figure 7 presents free-end angular displacement for normalized magnetic field strength $MBAL^2/E_{MR}I$. The dotted lines represent the results presented in Wang et al. [29] and the circle markers are the solutions for the present model (48). The free-end angular displacement has been plotted for various angles of the applied magnetic field (ϕ in figure 7). As the magnitude of applied magnetic field is increased, the free-end angle of the beam increases and finally saturates to a certain value ϕ, as the beam lines up with the external magnetic field. A distinctive result is obtained when $\phi = 180^o$, i.e. when the applied magnetic field is directly aligned with the beam. The free-end angle of the beam does not change for the first two experimental results. This is because the magnetic force acting on the beam along the beam orientation and not perpendicular to the beam. Therefore a purely compressive force is experienced by the beam and no lateral deviation is observed. However, this is an unstable equilibrium and therefore, once the applied magnetic field exceeds a certain value, the beam can overcome the energy barrier required to jump out of the unstable equilibrium and proceeds to experience lateral displacement.

The advantage of incorporating a hyperelastic constitutive equation into the theoretical model can be effectively seen when its compared with experimental results reported by *Zhao et al.* [5]. In the research conducted by *Zhao et al.*, the exact problem defined in figure 1 was studied by conducting experiments with varying magnitude of the applied magnetic field for different beam dimensions. The free-end angle was measured by varying the normalized flux density for 4 values of the beam dimension (L/H represents the ratio of the length versus height of the beam as represented in figure 2). The magnetic field is applied perpendicular to the initial beam

Journal Pre-proof

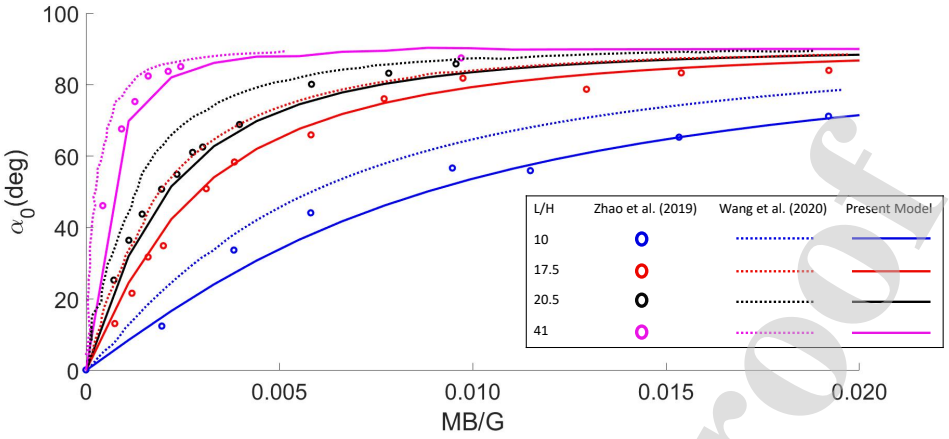

Figure 8: The graph presents the comparison between the experimental results, linear model and hyperelastic constitutive model when a constant magnetic field is applied perpendicular to a cantilever soft beam containing hard-magnetic particles. The end-angular displacement has been plotted against the normalized flux density MB/G for various geometric configurations (L/H, please refer to figure 2 for the notations).

direction (i.e. $\phi = 90^o$), which means the magnetic field is applied perpendicular to the beam. When $\phi = 90^o$, equation (48) gets simplified into

$$\frac{MB}{G}\left(\frac{L}{H}\right)^2 = \frac{(\Phi(\pi/2, \alpha_0))^2}{8} \tag{57}$$

where G is the shear modulus ($E_{MR} \approx 3G$), I is the second moment of the cross sectional area and H is the height of the beam's cross-section. The comparison between the experimental results, linear model [29] and hyperelastic model has been shown in figure 8. The end-angular displacement has been plotted against the normalized flux density MB/G for various geometric configurations (L/H). The magnetic field is applied at 90^o to the direction of initial magnetization vector ($\mathbf{M}$). It is visible from figure 8 that the model presented in this paper resonates with the experimental data more efficiently than the model formulated in *Wang et al.* [29]. This accuracy increase is due to the hyperelastic constitutive model and Prony series approximation of time dependent material properties. Furthermore, this effect can be more profoundly seen at lower L/H values. The assumption of the slender rod is valid at higher L/H ratios, which is why the Wang et al. model predicts the experimental results more accurately at $L/H = 41$. At $L/H = 10$, the prediction of the Wang et al. model is not quite the same as the experimental results presented in Zhao et al. However; it is clear from the graph (in figure 8) that the present model developed can capture the experimental results accurately for all beam dimensions. Therefore, incorporating the hyperelastic constitutive model for the elastic contribution of the Helmholtz energy increases the accuracy of the slender beam assumption to a wide range of the beam's dimensional configuration. Certain applications of the hard-magnetic soft beams as actuators and sensors require the deflection variation with respect to the applied magnetic to be gradual and not instantaneous. The variation of the free-end angle presented in figure 8, shows that this gradual behaviour is obtained at lower L/H ratios. Therefore, theoretical models need to predict this behaviour accurately. The present model fulfils this condition without loss of accuracy for other beam configurations.

Anticlastic bending will result in a gradient of stress patterns at each cross sectional area of the beam. The principal stress in the orthogonal directions are given by [49]

$$T_1 = T_2 = \frac{2}{\lambda^2\lambda_Z}\left\{(\lambda^2 - 1)a + ((\lambda^2 + \lambda_Z^2)\lambda^2 - 2)b + (\lambda^4\lambda_Z^2 - 1)c\right\} \tag{58}$$

$$T_3 = \frac{2}{\lambda^2\lambda_Z}\left\{(\lambda_Z^2 - 1)a + 2(\lambda^2\lambda_Z^2 - 1)b + (\lambda^4\lambda_Z^2 - 1)c\right\} \tag{59}$$

Journal Pre-proof

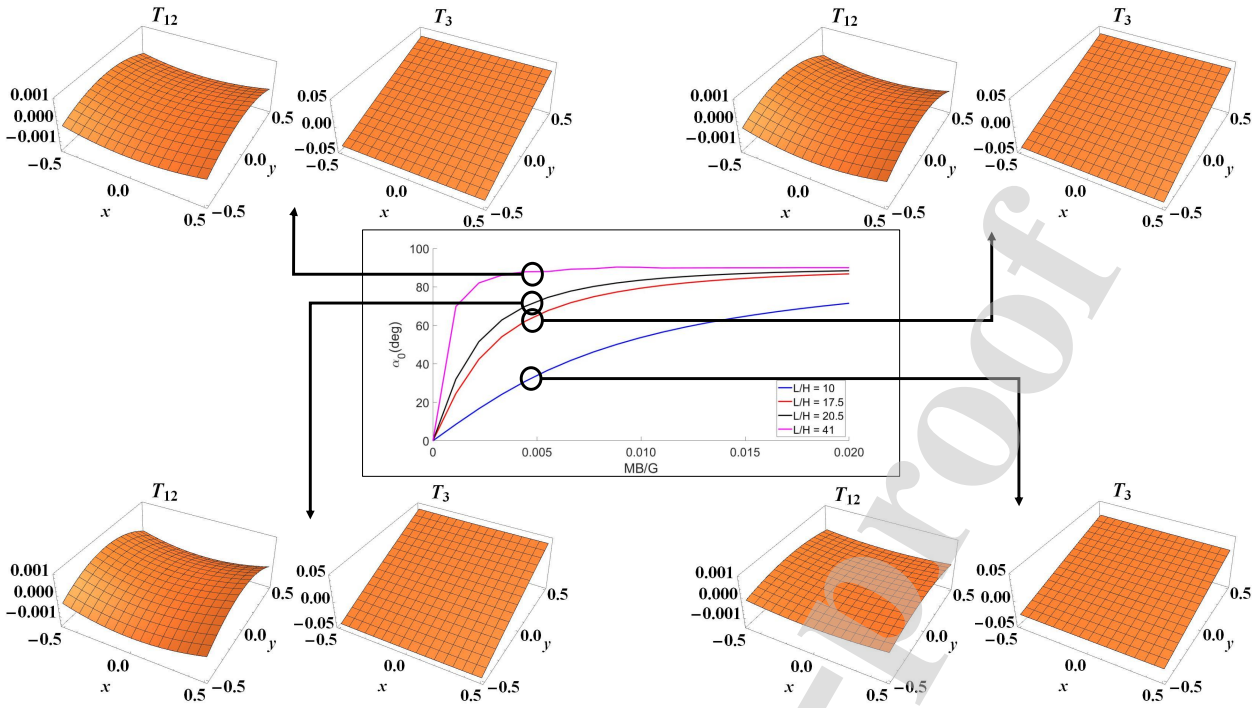

Figure 9: The image presents the stress profiles at various cross sections of the beam under a constant magnetic field. The value of the free-end angular displacement and normalized magnetic flux has been represented in the central graph. T_{12} represent the principal stresses in x and y direction and T_3 represents the principal stress in z direction.

where λ and λ_Z are the stretches in the X, Y and Z directions respectively. T_{12} represent the principal stresses in x and y direction and T_3 represents the principal stress in z direction. The cross sectional stress profiles arising due to the anticlastic bending have been represented in figure 9. Stress profiles have been plotted for 4 different beam dimensions. The value of the free-end angular displacement and normalized magnetic flux has been represented in the central graph. The normalized magnetic flux has been kept constant at 0.005 to point out the variation of the cross sectional principal stress with L/H ratio. The figure is just a representation of the cross sectional stresses arising due to anticlastic bending. Equation 59 can be used to essentially calculate the stresses at any point for any parameter value.

As pointed above, the soft materials used to synthesise hard-magnetic soft materials are usually polymeric hydrogels. Therefore, to simulate the viscous effects in there material using Prony series approximation, we can use the material properties of a polymeric hydrogel. The relaxation time of polydimethylacrylamide hydrogels is usually in the order of $\mathcal{O}(1s)$. The time dependent response of beam bending has been represented in figure 10. For a fixed normalized magnetic field, the free-end angular displacement decreases with time. As time increases, the material relaxes and its modulus decreases (or conversely increase in its compliance). From equation 50 we can see that the decrease in modulus results in a smaller deflection angle. However, this effect is less prominent at higher magnitudes of the magnetic field. Therefore, the free-end angular displacement does not change heavily with the applied magnetic field or due to the relaxation effect of the material properties at high normalized magnetic fields. The effect is prominent only at lower normalized values of the magnetic field. Figure 10 represents the free-end angle at varying magnitudes of magnetic fields at different time stamps for $\phi = 30^o$ and $\phi = 60^o$.

4. Conclusion

In this paper, we presented an analytical solution to a hard-magnetic hyperelastic soft beam under the influence of a constant magnetic field. The deformation in the perpendicular direction to the beam bending, caused by the Anticlastic effect was also considered. The principal stresses developed in the cross-sectional area were calculated. The time dependence of the material properties was modelled using a Prony series

Journal Pre-proof

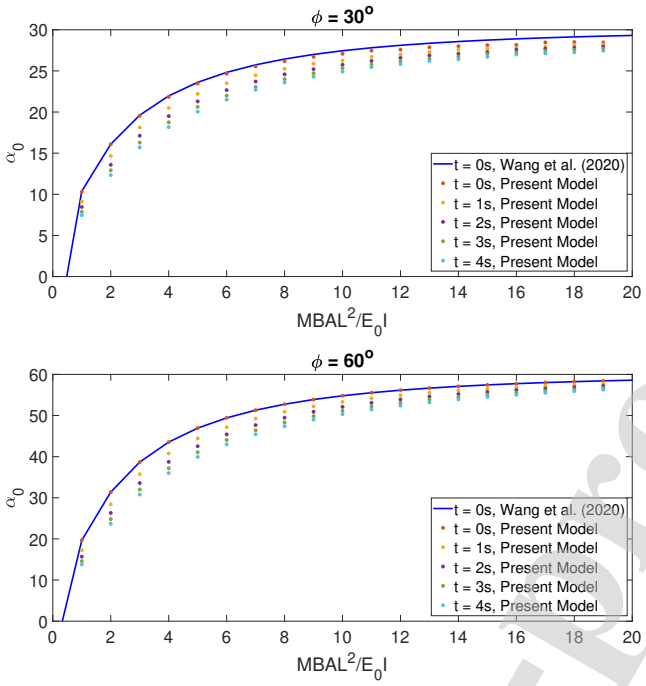

Figure 10: The image represents the beam bending angle (α_0) against normalized magnetic field with material degradation due to viscous effects. Wang et al. (2020) represents the experimental data represented in [29]. The numerical solution for α_0 has been shown for $\phi = 30^o$ and 60^o. All the notation are the same as given in equation 50. E_0 is the inverse of J_0, i.e. $E_0 = 1/J_0$.

approximation. The model was compared with previously conducted experimental, analytical and numerical results. The proposed model enables easier, faster and more accurate analysis of Hard-magnetic soft material as opposed to the previous studies. The authors would like to propose ideas for further research, where the assumption of a thin beam must be reduced. Moreover, future theoretical models must drop the assumption of all magnetic particles possessing a relative permeability close to 1. Furthermore, a thorough experimental study needs to be conducted to analyze the time dependent response of hyperelastic beam under the influence of magnetic fields.

5. Acknowledgements

A. Arockiarajan would like to acknowledge the Indian Institute of Technology Madras (IIT Madras) for providing financial aid under Project No. SB20210850MMMHRD008275 through the Institute of Eminence.

References

[1] K. Yu, A. Xin, Q. Wang, Mechanics of light-activated self-healing polymer networks, Journal of the Mechanics and Physics of Solids 124 (2019) 643–662. doi:https://doi.org/10.1016/j.jmps.2018.11.019.

[2] R. Bai, K. Bhattacharya, Photomechanical coupling in photoactive nematic elastomers, arXiv preprint arXiv:2002.04000 (2020). doi:https://doi.org/10.1016/j.jmps.2020.104115.

[3] K. Mehta, A. R. Peeketi, J. A. Sol, M. G. Debije, P. R. Onck, R. K. Annabattula, Modeling of surface waves in photo-responsive viscoelastic liquid crystal thin films under a moving light source, Mechanics of Materials (2020) 103388doi:https://doi.org/10.1016/j.mechmat.2020.103388.

[4] M. L. Dunn, K. Maute, Photomechanics of blanket and patterned liquid crystal elastomer films, Mechanics of materials 41 (10) (2009) 1083–1089. doi:https://doi.org/10.1016/j.mechmat.2009.06.004.

Journal Pre-proof

[5] R. Zhao, Y. Kim, S. A. Chester, P. Sharma, X. Zhao, Mechanics of hard-magnetic soft materials, Journal of the Mechanics and Physics of Solids 124 (2019) 244–263. doi:https://doi.org/10.1016/j.jmps.2018.10.008.

[6] P. V. Rao, S. Maniprakash, S. Srinivasan, A. Srinivasa, Functional behavior of isotropic magnetorheological gels, Smart materials and structures 19 (8) (2010) 085019. doi:https://doi.org/10.1088/0964-1726/19/8/085019.

[7] P. Saxena, J.-P. Pelteret, P. Steinmann, Modelling of iron-filled magneto-active polymers with a dispersed chain-like microstructure, European Journal of Mechanics-A/Solids 50 (2015) 132–151. doi:https://doi.org/10.1016/j.euromechsol.2014.10.005.

[8] G. Kocak, C. Tuncer, V. Bütün, ph-responsive polymers, Polymer Chemistry 8 (1) (2017) 144–176. doi:https://doi.org/10.1039/C6PY01872F.

[9] S. Dai, P. Ravi, K. C. Tam, ph-responsive polymers: synthesis, properties and applications, Soft Matter 4 (3) (2008) 435–449. doi:https://doi.org/10.1039/B714741D.

[10] F. Vogel, S. Göktepe, P. Steinmann, E. Kuhl, Modeling and simulation of viscous electro-active polymers, European Journal of Mechanics - A/Solids 48 (2014) 112 – 128, frontiers in Finite-Deformation Electromechanics. doi:https://doi.org/10.1016/j.euromechsol.2014.02.001.
URL http://www.sciencedirect.com/science/article/pii/S099775381400014X

[11] W. Kim, M. Taya, M. Nguyen, Electrical and thermal conductivities of a silver flake/thermosetting polymer matrix composite, Mechanics of Materials 41 (10) (2009) 1116–1124. doi:https://doi.org/10.1016/j.mechmat.2009.05.009.

[12] W. Zhao, L. Liu, J. Leng, Y. Liu, Thermo-mechanical behavior prediction of shape memory polymer based on the multiplicative decomposition of the deformation gradient, Mechanics of Materials 143 (2020) 103263. doi:https://doi.org/10.1016/j.mechmat.2019.103263.

[13] M. Zare, M. P. Prabhakaran, N. Parvin, S. Ramakrishna, Thermally-induced two-way shape memory polymers: Mechanisms, structures, and applications, Chemical Engineering Journal 374 (2019) 706–720. doi:https://doi.org/10.1016/j.cej.2019.05.167.

[14] M. Baniasadi, E. Yarali, A. Foyouzat, M. Baghani, Crack self-healing of thermo-responsive shape memory polymers with application to control valves, filtration, and drug delivery capsule, European Journal of Mechanics-A/Solids 85 104093. doi:https://doi.org/10.1016/j.euromechsol.2020.104093.

[15] M. Mehnert, M. Hossain, P. Steinmann, Towards a thermo-magneto-mechanical coupling framework for magneto-rheological elastomers, International Journal of Solids and Structures 128 (2017) 117–132. doi:https://doi.org/10.1016/j.ijsolstr.2017.08.022.

[16] A. K. Bastola, M. Hossain, A review on magneto-mechanical characterizations of magnetorheological elastomers, Composites Part B: Engineering (2020) 108348doi:https://doi.org/10.1016/j.compositesb.2020.108348.

[17] G. Paradossi, F. Cavalieri, E. Chiessi, C. Spagnoli, M. K. Cowman, Poly (vinyl alcohol) as versatile biomaterial for potential biomedical applications, Journal of Materials Science: Materials in Medicine 14 (8) (2003) 687–691.

[18] R. Zabihyan, J. Mergheim, J. Pelteret, B. Brands, P. Steinmann, Fe2 simulations of magnetorheological elastomers: influence of microscopic boundary conditions, microstructures and free space on the macroscopic responses of mres, International Journal of Solids and Structures 193 (2020) 338–356. doi:https://doi.org/10.1016/j.ijsolstr.2020.02.015.

[19] D. Pivovarov, P. Steinmann, On stochastic fem based computational homogenization of magneto-active heterogeneous materials with random microstructure, Computational Mechanics 58 (6) (2016) 981–1002. doi:https://doi.org/10.1007/s00466-016-1329-4.

Journal Pre-proof

[20] M. Hossain, P. Saxena, P. Steinmann, Modelling the curing process in magneto-sensitive polymers: rate-dependence and shrinkage, International Journal of Non-Linear Mechanics 74 (2015) 108–121. doi:https://doi.org/10.1016/j.ijnonlinmec.2015.04.008.

[21] P. Saxena, M. Hossain, P. Steinmann, Nonlinear magneto-viscoelasticity of transversally isotropic magneto-active polymers, Proceedings of the Royal Society A: Mathematical, Physical and Engineering Sciences 470 (2166) (2014) 20140082. doi:https://doi.org/10.1098/rspa.2014.0082.

[22] D. Kumar, S. Sarangi, Electro-magnetostriction under large deformation : Modeling with experimental validation, Mechanics of Materials 128 (2019) 1 – 10. doi:https://doi.org/10.1016/j.mechmat.2018.10.001.

[23] B. L. Walter, J.-P. Pelteret, J. Kaschta, D. W. Schubert, P. Steinmann, Preparation of magnetorheological elastomers and their slip-free characterization by means of parallel-plate rotational rheometry, Smart Materials and Structures 26 (8) (2017) 085004. doi:https://doi.org/10.1088/1361-665X/aa6b63.

[24] B. Walter, P. Saxena, J. Kaschta, D. W. Schubert, P. Steinmann, Magneto-sensitive elastomers: An experimental point of view, PAMM 14 (1) (2014) 403–404. doi:10.1002/pamm.201410189.

[25] Y. Kim, H. Yuk, R. Zhao, S. A. Chester, X. Zhao, Printing ferromagnetic domains for untethered fast-transforming soft materials, Nature 558 (7709) (2018) 274–279. doi:https://doi.org/10.1038/s41586-018-0185-0.

[26] L. Borcea, O. Bruno, On the magneto-elastic properties of elastomer–ferromagnet composites, Journal of the Mechanics and Physics of Solids 49 (12) (2001) 2877–2919. doi:https://doi.org/10.1016/S0022-5096(01)00108-9.

[27] M. Zrínyi, L. Barsi, A. Büki, Deformation of ferrogels induced by nonuniform magnetic fields, The Journal of chemical physics 104 (21) (1996) 8750–8756. doi:https://doi.org/10.1063/1.471564.

[28] D. Garcia-Gonzalez, Magneto-visco-hyperelasticity for hard-magnetic soft materials: theory and numerical applications, Smart Materials and Structures 28 (8) (2019) 085020. doi:https://doi.org/10.1088/1361-665X/ab2b05.

[29] L. Wang, Y. Kim, C. F. Guo, X. Zhao, Hard-magnetic elastica, Journal of the Mechanics and Physics of Solids (2020) 104045doi:https://doi.org/10.1016/j.jmps.2020.104045.

[30] G. Z. Lum, Z. Ye, X. Dong, H. Marvi, O. Erin, W. Hu, M. Sitti, Shape-programmable magnetic soft matter, Proceedings of the National Academy of Sciences 113 (41) (2016) E6007–E6015. doi:https://doi.org/10.1073/pnas.1608193113.

[31] M. Runciman, A. Darzi, G. P. Mylonas, Soft robotics in minimally invasive surgery, Soft robotics 6 (4) (2019) 423–443. doi:https://doi.org/10.1089/soro.2018.0136.

[32] M. Cianchetti, C. Laschi, A. Menciassi, P. Dario, Biomedical applications of soft robotics, Nature Reviews Materials 3 (6) (2018) 143–153. doi:10.1038/s41578-018-0022-y.

[33] G.-Z. Yang, J. Bellingham, P. E. Dupont, P. Fischer, L. Floridi, R. Full, N. Jacobstein, V. Kumar, M. McNutt, R. Merrifield, et al., The grand challenges of science robotics, Science robotics 3 (14) (2018) eaar7650. doi:10.1126/scirobotics.aar7650.

[34] Y.-H. Pao, Electromagnetic forces in deformable continua, In: Mechanics today. Volume 4.(A78-35706 14-70) New York 4 (1978) 209–305.

[35] A. C. Eringen, G. A. Maugin, Electrodynamics of continua I, Springer-Verlag New York, 1990.

[36] G. A. Maugin, Continuum mechanics of electromagnetic solids, Elsevier, 1989.

[37] I. Brigadnov, A. Dorfmann, Mathematical modeling of magneto-sensitive elastomers, International Journal of Solids and Structures 40 (18) (2003) 4659–4674. doi:https://doi.org/10.1016/S0020-7683(03)00265-8.

Journal Pre-proof

[38] A. Dorfmann, R. Ogden, Nonlinear magnetoelastic deformations of elastomers, Acta Mechanica 167 (1) (2004) 13–28. doi:https://doi.org/10.1007/s00707-003-0061-2.

[39] P. Saxena, M. Hossain, P. Steinmann, A theory of finite deformation magneto-viscoelasticity, International Journal of Solids and Structures 50 (24) (2013) 3886–3897. doi:https://doi.org/10.1016/j.ijsolstr.2013.07.024.

[40] D. Garcia-Gonzalez, C. M. Landis, Magneto-diffusion-viscohyperelasticity for magneto-active hydrogels: rate dependences across time scales, Journal of the Mechanics and Physics of Solids (2020) 103934doi:10.1016/j.jmps.2020.103934.

[41] P. J. Flory, Principles of polymer chemistry, Cornell University Press, 1953.

[42] Y. Kim, G. A. Parada, S. Liu, X. Zhao, Ferromagnetic soft continuum robots, Science Robotics 4 (33) (2019). doi:10.1126/scirobotics.aax7329.

[43] W. Chen, Z. Yan, L. Wang, On mechanics of functionally graded hard-magnetic soft beams, International Journal of Engineering Science 157 (2020) 103391. doi:https://doi.org/10.1016/j.ijengsci.2020.103391.

[44] L. Lanzoni, A. M. Tarantino, The bending of beams in finite elasticity, Journal of Elasticity 139 (1) (2020) 91–121. doi:https://doi.org/10.1007/s10659-019-09746-8.

[45] C. Truesdell, W. Noll, The non-linear field theories of mechanics, in: The non-linear field theories of mechanics, Springer, 2004, pp. 1–579. doi:10.1007/978-3-662-10388-3.

[46] F. Falope, L. Lanzoni, A. Tarantino, Bending device and anticlastic surface measurement of solids under large deformations and displacements, Mechanics Research Communications 97 (2019) 52–56. doi:https://doi.org/10.1016/j.mechrescom.2019.04.011.

[47] A. Ferguson, J. P. Andrews, An experimental study of the anticlastic bending of rectangular bars of different cross-sections, Proceedings of the Physical Society 41 (1) (1928) 1. doi:10.1088/0959-5309/41/1/301.

[48] G. H. Lee, I. H. Stockel, A study of the anticlastic bending in elastic plates and bars, US Naval Postgraduate School, 1951.

[49] L. Lanzoni, A. M. Tarantino, Finite anticlastic bending of hyperelastic solids and beams, Journal of Elasticity 131 (2) (2018) 137–170. doi:https://doi.org/10.1007/s10659-017-9649-y.

[50] A. Rajan, R. Pramanik, A. Narayanan, A. Arockiarajan, Mechanics of viscoelastic buckling in slender hydrogels, Materials Research Express 6 (5) (2019) 055320. doi:https://doi.org/10.1088/2053-1591/ab0691.

[51] D. Panda, S. Konar, S. K. Bajpai, A. Arockiarajan, Synthesis and viscoelastic characterization of microstructurally aligned silk fibroin sponges, Journal of the mechanical behavior of biomedical materials 71 (2017) 362–371. doi:https://doi.org/10.1016/j.jmbbm.2017.03.029.

[52] R. Pramanik, B. Ganivada, F. Ram, K. Shanmuganathan, A. Arockiarajan, Influence of nanocellulose on mechanics and morphology of polyvinyl alcohol xerogels, Journal of the mechanical behavior of biomedical materials 90 (2019) 275–283. doi:https://doi.org/10.1016/j.jmbbm.2018.10.024.

[53] R. Pramanik, A. Arockiarajan, Influence of mechanical compressive loads on microstructurally aligned pva xerogels, Materials Letters 236 (2019) 222–224. doi:https://doi.org/10.1016/j.matlet.2018.10.073.

[54] D. M. Knapp, V. H. Barocas, A. G. Moon, K. Yoo, L. R. Petzold, R. T. Tranquillo, Rheology of reconstituted type i collagen gel in confined compression, Journal of Rheology 41 (5) (1997) 971–993. doi:https://doi.org/10.1122/1.550817.

[55] M. H. R. Ghoreishy, Determination of the parameters of the prony series in hyper-viscoelastic material models using the finite element method, Materials & Design 35 (2012) 791–797.

Journal Pre-proof

Highlights

- An analytical solution for the bending of hard-magnetic soft beam has been derived
- Mooney-Rivlin model has been used to capture the non-linearity of the material
- Coupled anticlastic bending has also been incorporated into the framework
- Prony series approximation was used to encapsulate the time-dependent response

Journal Pre-proof

Journal Pre-proof

Author Agreement Statement

We the undersigned declare that this manuscript is original, has not been published before and is not currently being considered for publication elsewhere. We confirm that the manuscript has been read and approved by all named authors and that there are no other persons who satisfied the criteria for authorship but are not listed. We further confirm that the order of authors listed in the manuscript has been approved by all of us. We understand that the Corresponding Author is the sole contact for the Editorial process. He is responsible for communicating with the other authors about progress, submissions of revisions and final approval of proofs.

Aakila Rajan	Conceptualization; Methodology;Data curation; Formal analysis; Investigation; Resources; Visualization; Roles/Writing - original draft; Writing - review & editing.
A. Arockiarajan	Methodology; Project administration; Funding acquisition; Validation; Writing - review & editing

Signed by all authors as follows:

Aakila Rajan.
Aakila Rajan
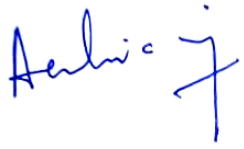
Arockiarajan

Journal Pre-proof

Declaration of interests

☒ The authors declare that they have no known competing financial interests or personal relationships that could have appeared to influence the work reported in this paper.

☐The authors declare the following financial interests/personal relationships which may be considered as potential competing interests:

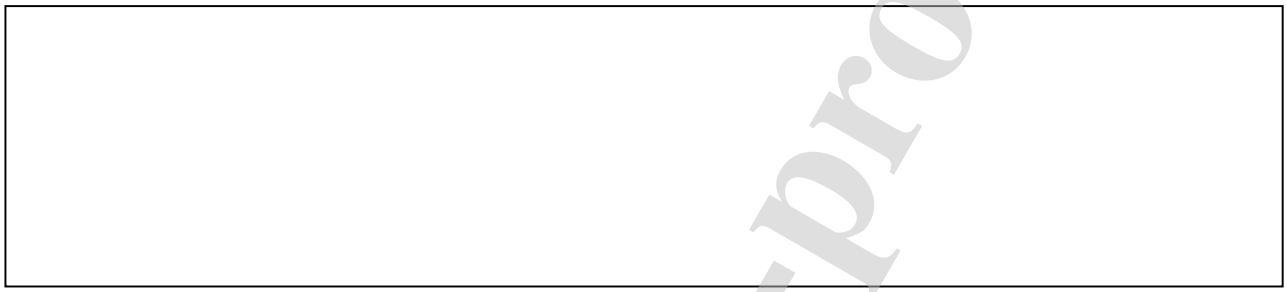

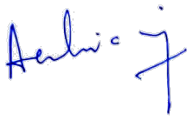

Arockiarajan

Aakila Rajan

Journal Pre-proof